

©2024 IEEE. Personal use of this material is permitted. Permission from IEEE must be obtained for all other uses, in any current or future media, including reprinting/republishing this material for advertising or promotional purposes, creating new collective works, for resale or redistribution to servers or lists, or reuse of any copyrighted component of this work in other works. DOI: <https://doi.org/10.1109/MCE.2024.3387019>

Unsupervised explainable activity prediction in competitive Nordic Walking from experimental data

Silvia García-Méndez

Francisco de Arriba-Pérez

Francisco J. González-Castaño

Information Technologies Group, atlanTTic, University of Vigo

Javier Vales-Alonso

Communication and Information Technologies Department,
Technical University of Cartagena

Abstract—Artificial Intelligence (AI) has found application in Human Activity Recognition (HAR) in competitive sports. To date, most Machine Learning (ML) approaches for HAR have relied on offline (batch) training, imposing higher computational and tagging burdens compared to online processing unsupervised approaches. Additionally, the decisions behind traditional ML predictors are opaque and require human interpretation. In this work, we apply an online processing unsupervised clustering approach based on low-cost wearable Inertial Measurement Units (IMUs). The outcomes generated by the system allow for the automatic expansion of limited tagging available (e.g., by referees) within those clusters, producing pertinent information for the explainable classification stage. Specifically, our work focuses on achieving automatic explainability for predictions related to athletes' activities, distinguishing between correct, incorrect, and cheating practices in Nordic Walking. The proposed solution achieved performance metrics of close to 100 % on average.

INTRODUCTION

Automatic Human Activity Recognition (HAR) [1], [2] is a field of great interest for sports research. HAR is based on the premise that body movements produce differentiated patterns of signals that can be collected with sensors such as visual recognition and Inertial Measurement Units (IMUs).

Sensors in the literature on sport HAR can be broadly divided into three groups: (i) portable devices or wearables (e.g., gyroscopes and accelerometers), (ii) environmental sensors (e.g., cameras and GPS), and (iii) sensors integrated into personal terminals (e.g., smartphones). Integrated sensors are popular and allow

for app-based business models, but wearable sensors are preferred for stringent scenarios that require freedom of movement [3]–[5], as it is often the case with sports practice [6].

Current methodologies to evaluate sports performance involve predictive techniques based on statistical methods. Performance in this setting, however, is the joint result of a wide variety of factors, including level of training, physical condition, and team interactions [7]. More complex, intelligent, methodologies are therefore needed to characterize, beyond performance, specific states during the practice of sport or to predict certain events that may lead to injuries [8].

These emerging needs have led to the application of Artificial Intelligence (AI) such as Machine Learn-

ing (ML) [9]. Nevertheless, decisions made by traditional ML predictors are opaque and require human interpretation of the reasons underlying the decisions. This work focuses on explainable AI (XAI), a relatively unexplored field in the area of sport. XAI techniques are designed to infer the reasons behind prediction outcomes¹. In this study, we leverage XAI to provide automatic interpretations and explanations of the differentiation between correct, incorrect, and cheating practices in a Nordic Walking case study using low-cost IMUs. On a more detailed level, we analyze and leverage the most relevant features of the ML model to improve explainability.

The rest of this paper is organized as follows. The section RELATED WORK reviews relevant work on HAR in sports using supervised and unsupervised ML techniques. The section METHODOLOGY describes the solution for explainable unsupervised characterization of Nordic Walking practice. The section EXPERIMENTAL RESULTS presents the experimental data and implementations used and the results obtained. Finally, the section CONCLUSIONS provides overall discussion and highlights the future scope of research and study.

RELATED WORK

Numerous research works in the field of sport have analyzed action and movement [9] as well as fitness and performance [10]. Many of these studies use low-cost commercial IMUs, such as accelerometers, gyroscopes, and magnetometers. Examples of outputs measured include basketball movements [11], tennis and table tennis strokes [12], and volleyball training [13].

The more recent ML solutions employ big-data and small-data models. Big-data models are typically deep learning models due to the large volumes of data involved [14], [15]. However, data volumes in sports training scenarios are generally small, corresponding to a single individual and even a single training session. Unfortunately, supervised approaches have dominated in HAR [16].

Supervised methodologies for the analysis of sports practice include Decision Trees (DT) [17], Support Vector Machines (SVM) [18], k -nearest neighbors (k -NN) [19], and ensemble methods such as boosting, bagging, and stacking [20]. Notably, Noor *et al.* (2017) [21] differentiated between transitional

and non-transitional activities. In contrast, Bulbul *et al.* (2018) [22] recognized six activities: walking, climbing up and down stairs, sitting, standing, and lying down. Zainudin *et al.* (2018) [23] combined one-versus-all (OVA) models with a self-adaptive algorithm to select features for sports practice analysis. In addition, Bharti *et al.* (2019) [24] studied different body sensor locations on the extremities for activity recognition. Gil-Martin *et al.* (2020) [25] applied deep learning models to annotated data to identify movements during activity, while Zhu *et al.* (2020) [26] predicted athlete performance using an SVM model. Adopting a different approach, Rossi *et al.* (2021) [27] studied injury prevention during training, and Webber & Rojas (2021) [28] fused data from accelerometer and gyroscope sensors at sensor, feature, and decision levels to apply diverse well-known ML models (DT, k -NN, Linear Discriminant Analysis (LDA) and SVM). Although the best results were obtained with decision-level fusion, the authors concluded that the computational power and processing times required were unacceptable for a practical HAR system. Zeng *et al.* (2021) [29] predicted effort levels during the execution of physical activities using acceleration and angular velocity sensors on the arms, waist, and wrists. Finally, Zhang & Li (2022) [30] used neural networks and SVMs to analyze athlete movements and the impact of training equipment.

Unsupervised ML techniques [31], which, when applicable, are highly convenient as they do not require manual tagging and can be used to detect practice patterns. However, *a priori*, a specific pattern may be complex to assign to a specific state (*i.e.*, sports execution phase). There are few works on unsupervised ML techniques in sports. Domingo *et al.* (2018) [32] applied Subsequence Time Series (STS) analysis of dominant arm acceleration data using K -means clustering [33], while Gu *et al.* (2018) [34] proposed temporarily grouping large volumes of unlabeled data into duly annotated time points. Conversely, Van Kuppevelt *et al.* (2019) [35] applied an unsupervised Hidden Semi-Markov Model to automatically segment and cluster data from wearable acceleration sensors to infer the type of activity performed from the clusters detected. Finally, Janarthanan *et al.* (2020) [36] employed an unsupervised deep learning-assisted reconstructed encoder for sports activity recognition, while Serantoni *et al.* (2022) [37] used a K -means model to differentiate between overexertion stages in cardiovascular exercise.

Nordic Walking involves complex interactions be-

¹Available at <https://doi.org/10.48550/arXiv.2302.05624>, March 2024.

tween various body parts. When performed incorrectly, it increases the risk of injury and reduces training effectiveness. A typical observable error in Nordic Walking, for example, is dragging the tips of the poles over the ground [38]. To prevent cheating, in Nordic Walking competitions, judges positioned along the track evaluate whether participants are purposely using incorrect techniques, such as when running instead of walking. Some works on automatic activity monitoring based on integrated pole sensors, heart sensors, and GPS data [39], [40] have used static formulae, that is, formulae not involving multivariate or intelligent data analysis such as ML. One clear exception is the work by Derungs *et al.* (2018) [38], which proposed a supervised regression system to detect incorrect practices based on IMUs placed in seven fixed body locations. Wiktorski *et al.* (2019) [41] employed Dynamic Time Warping (DTW) and a semi-supervised approach to differentiate between Nordic Walking and other activities. This is the only example to our knowledge of the application of a, to an extent, unsupervised technique to this sport.

Finally, and particularly relevant to the scope of this work, it should be noted that XAI [42], which has been applied to a wide range of applications [43], [44], is largely missing in elite sports [45], with a few exceptions based on strictly offline (batch) supervised solutions. Examples include explainable game-play prediction [46] and case-based reasoning to recommend training plans to marathon runners using a visual dashboard [47]. Sun *et al.* (2020) [48] studied the trade-off between accuracy and transparency in sports analytics. They employed a tree version of a neural network to generate visual (not natural language) descriptions of ice hockey and soccer practice predictions. Finally, Lisca *et al.* (2021) [49] applied an extreme gradient boosting ensemble model in batch mode to obtain symbolic insights into goalkeeper kinematics from a single motion sensor.

RESEARCH CONTRIBUTION

To the best of our knowledge, the solution is the first work in sport HAR that applies explainability techniques to infer knowledge from unsupervised small-data analysis in online processing mode, taking Nordic Walking as a case study. Unlike batch processing, online processing updates model profiling and classification with each incoming sample [50]. Therefore, the system can be easily deployed in the field without imposing a manual burden on operators.

A generalistic supervised HAR system must be trained in advance. This is a huge, costly, and laborious undertaking involving many practitioners. That said, there is a finite known set of well-defined practice patterns in certain sports, both in training and competition scenarios. This is the case with Nordic Walking, where these well-defined patterns include correct practice, cheating, and, in the case of coaching, incorrect practices. We demonstrate that it is possible to cluster these patterns very efficiently, to a level comparable to that seen with supervised systems. Then, with minimal burden, it is possible to label just some data samples within each cluster. This would be a quite natural process in Nordic Walking competitions. Judges could easily tag these references during a race by clicking a button when a practitioner passes by their locations. Finally, once the labels are propagated within their respective clusters, the data could be re-classified for explainability. It should be noted that *the idea of this re-classification is not to improve classification performance* (since the clustering stage has already classified the data samples by propagating reference labels) but to apply a supervised tree classification method that, unlike clustering, is *intrinsically explainable*. Accordingly, we ultimately achieve classification at no tagging cost and produce useful explainability information.

The base clustering technique, which generates the labels for the explainability classification stage by expanding the limited *a posteriori* tagging available within the clusters, achieves up to 97.68 % accuracy. Supervised learning is only applied in this research for two purposes: (i) as previously explained, to extract the relevant features for the explainability module with minimal labor, and (ii) as a baseline for the comparisons in the experimental evaluation. Summing up, unsupervised clustering enables automatic tagging expansion, a solution to a prevalent challenge in commercial HAR [51]. This feature is subsequently leveraged to train an automatically supervised classifier for explainability purposes at minimal cost.

HAR is of great interest to consumer electronics in sports and health [52]–[54]. Some representative examples of commercial products are Fibaro², Fitbit³, and Mi Band⁴. The target consumers of a commercial version of our system, rather than individual practition-

²Available at <https://www.fibaro.com>, March 2024.

³Available at <https://www.fitbit.com>, March 2024.

⁴Available at <https://www.mi.com/global/miband>, March 2024.

ers, would be group coaches, course organizers, small event organizers, and similar. The implementation could be based on low-cost consumer electronics using smartphones and compact accelerometers as described in the EXPERIMENTAL RESULTS section.

Table 1 provides a brief comparison of our work with most of the related previous works discussed in this section.

METHODOLOGY

Figure 1 shows the scheme of the solution. It comprises the IMUs (with accelerometers, gyroscopes, and magnetometers) placed on wrists, ankles, and poles; a data processing module composed of data calibration, feature engineering and analysis & selection stages; and an online processing clustering module, whose outcome is compared with a supervised classification baseline. Moreover, the automatically expanded labels from the unsupervised clustering module train a supervised classifier for explainability purposes. Finally, the explainability module provides visual and natural language descriptions of the prediction outcome (*i.e.*, correct, cheating, or incorrect practices).

WEARABLE SENSORS

Three pairs of wearable IMUs are placed on the left and right sides of the body ($P = \{left, right\}$), specifically, on wrists, ankles, and poles ($L = \{wrist, ankle, pole\}$). Each IMU includes tri-axial ($A = \{x, y, z\}$) accelerometers (to capture the modulus and direction of the movement accelerations), gyroscopes (to capture the axis rotation speeds), and magnetometers (to capture the modulus and direction of the magnetic fields) ($S = \{accelerometer, gyroscope, magnetometer\}$), placed as shown in Figure 2. These IMUs gather movement data from the athletes. According to Edwards *et al.* (2019) [55], the maximum average acceleration in human walking is 4.5 g, so the operation range of the wearable sensors must cover this with a reasonable excess margin without compromising sensitivity.

The real-time data from the sensors is used as the input data for the data processing, online processing ML clustering, and explainability modules. Of interest to consumer electronics is that, even though the sensors are positioned in specific locations on the poles and the body, precise placement relative to body parts is unnecessary. Our tests showed significant linear and angular displacements of the sensors between and

during sessions, even within the same user. No special care was taken when strapping sensors into place during the data-gathering process.

DATA CALIBRATION, FEATURE ENGINEERING, ANALYSIS & SELECTION

During the data processing stage, raw data gathered by the wearable sensors are merged and filtered to ensure high-quality classification and explainability results. There are two fundamental data processing stages: first data calibration, and then, online processing feature engineering and analysis & selection.

Data calibration. Noise is a major issue when working with analogical signals. HAR signals are typically filtered using Finite Impulse Response (FIR) filters [56], [57]. In this work, we apply an averaging FIR filter and produce other features using four sliding windows of different sizes.

Different window lengths are set at the calibration stage by inspecting the sample intervals between successive minima of the sensor signals. To guarantee that at least two minima are captured per sensor, and given the repetitive limb and pole movements in Nordic Walking, the calibration stage lasts for 90 seconds. Let k be the size of the calibration stage in samples. For each sensor signal $x_{p,a,s,l}$, we define $v_{p,a,s,l}$ as follows (we will avoid the p, a, s, l sub-indices for clarity unless strictly necessary to explain the formulae):

Let v_1, v_2 be sample indexes in $[1, k - 1]$, and V_{aux} a subset of sample indexes, such that (1):

$$\begin{aligned} V_{aux} &= \{n \in [1, k - 1] \mid \\ &x[n - 1] > x[n] < x[n + 1]\} \\ v_1 &= \min(V_{aux}) \quad (1) \\ v_2 &= \min(V_{aux} \setminus \{v_1\}) \\ v &= v_2 - v_1 \end{aligned}$$

That is, $v_{p,a,s,l}$ is approximately the number of samples between the first two local minima delimiting an $x_{p,a,s,l}$ activity interval in the calibration stage. Let $V = \{v_{p,a,s,l}\}$, $|V| = |P| \times |A| \times |S| \times |L|$, and let $V' = \{v'_0, \dots, v'_{|V|-1}\}$, $v'_0 \leq v'_1 \leq \dots \leq v'_{|V|-1}$

Table 1. Comparison with previous research on intelligent analysis of Nordic Walking practice.

Authorship	Approach	Stream (online) processing	Explainability
Mocera <i>et al.</i> (2018) [39]	Rules & formulas	X	X
Pierleoni <i>et al.</i> (2022) [40]		X	X
Derungs <i>et al.</i> (2018) [38]	Supervised ML	X	X
Wiktorski <i>et al.</i> (2019) [41]	Semi-supervised ML	X	X
Our solution	Unsupervised ML	✓	✓

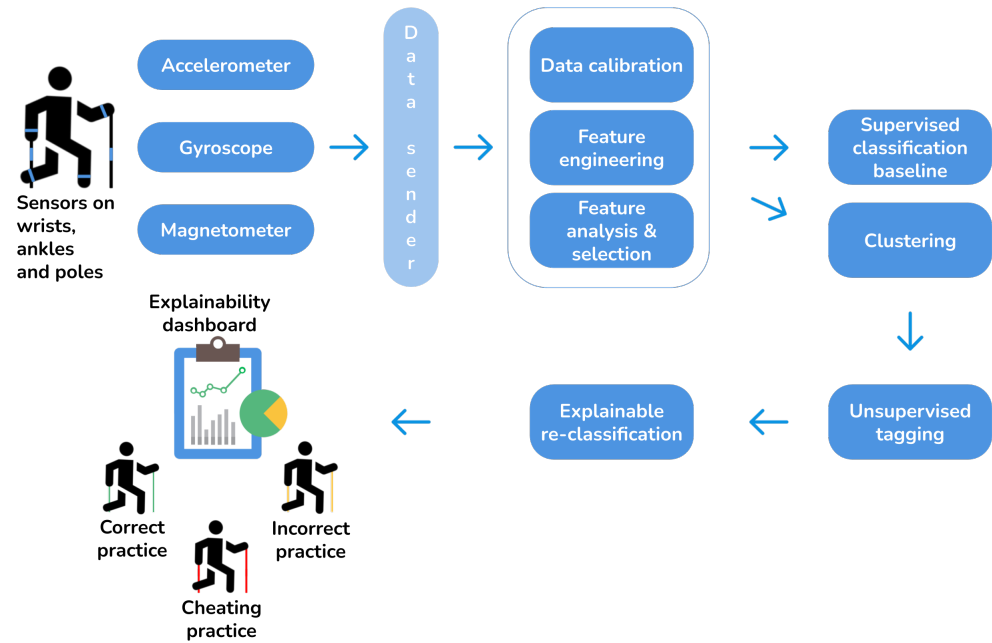


Figure 1. Nordic Walking practice assessment scheme.



Figure 2. Arrangement of the IMUs. A) positions on body and poles, B) wrist IMU, C) ankle IMU, D) pole IMUs, E) IMU size in cm.

be a sequence of reordered indexes of V , that is, $\forall v \in V, v \in V'$, in increasing order. Then, the four window lengths w_{Q1} , w_{Q2} , w_{Q3} and w_{avg} for all sensors are defined as follows (2), where r_{min} and r_{max} are the minimum and maximum data rates for all sensors used:

$$\begin{aligned} w_{Q1} &= \lfloor 2 \frac{r_{max}}{r_{min}} \rfloor v'_{\lfloor \frac{1}{4}|V| \rfloor} \\ w_{Q2} &= \lfloor 2 \frac{r_{max}}{r_{min}} \rfloor v'_{\lfloor \frac{2}{4}|V| \rfloor} \\ w_{Q3} &= \lfloor 2 \frac{r_{max}}{r_{min}} \rfloor v'_{\lfloor \frac{3}{4}|V| \rfloor} \\ w_{avg} &= \lfloor 2 \frac{r_{max}}{r_{min}} \rfloor \lfloor \frac{1}{|V|} \sum_{i=0}^{|V|} v'_i \rfloor \end{aligned} \quad (2)$$

Feature engineering. Once the sliding windows are selected, online processed features can be calculated $\forall n > \max(w_{Q1}, w_{Q2}, w_{Q3}, w_{avg})$ (to avoid a cold start) for each sensor $x_{p,a,s,l}$ and window size w : average ($avg_{p,a,s,l}^w$), standard deviation ($std_{p,a,s,l}^w$), quartile values ($Q_{1,p,a,s,l}^w$ - $Q_{3,p,a,s,l}^w$) and maximum modulus of the components of the Fast Fourier Transform (FFT) ($F_{p,a,s,l}^w$), as follows (3):

$$\forall w \in \{w_{Q1}, w_{Q2}, w_{Q3}, w_{avg}\}, \forall n \geq \{w, k\}$$

$$\begin{aligned} X[n] &= \{x[n-w+1], \dots, x[n]\}. \\ Y[n] &= \{y_0[n], y_1[n], \dots, y_{w-1}[n]\} | \\ & y_0[n] \leq y_1[n] \leq \dots \leq y_{w-1}[n], \\ & \text{where } \forall x \in X[n], x \in Y[n]. \end{aligned}$$

$$\begin{aligned} Q_1^w[n] &= y_{\lfloor \frac{1}{4}w \rfloor}[n] \\ Q_2^w[n] &= y_{\lfloor \frac{2}{4}w \rfloor}[n] \\ Q_3^w[n] &= y_{\lfloor \frac{3}{4}w \rfloor}[n] \\ avg^w[n] &= \frac{1}{w} \sum_{i=0}^w y_i[n] \\ std^w[n] &= \sigma(X[n]) \\ F^w[n] &= |FFT(X[n])|_{\infty} \end{aligned} \quad (3)$$

Feature analysis & selection.

Let $t_{\sigma} > 0$ be a configurable threshold, and Φ a transformation operator such that

$\Phi(\{x\}) = \{x\}$ if $x > t_{\sigma}$, $\Phi(\{x\}) = \emptyset$ otherwise. At any slot n , $n \geq k$, by considering the online processed standard deviations of all possible features at that moment, the set of selected features $S_{p,a,s,l}^w[n]$ for online processing prediction and training update at that slot is composed of $\Phi(\sigma(\{avg_{p,a,s,l}^w[k], \dots, avg_{p,a,s,l}^w[n]\})), \Phi(\sigma(\{std_{p,a,s,l}^w[k], \dots, std_{p,a,s,l}^w[n]\})), \Phi(\sigma(Q_{i,p,a,s,l}^w[k], \dots, Q_{i,p,a,s,l}^w[n])), i = 1, 2, 3, \text{ and } \Phi(\sigma(\{F_{p,a,s,l}^w[k], \dots, F_{p,a,s,l}^w[n]\})).$

ONLINE PROCESSING

Incremental profiling is performed at each slot n , using the set of features $S_{p,a,s,l}^w[n]$. Incremental classification is composed of a number of steps, described below.

ONLINE CLUSTERING AND UNSUPERVISED TAGGING

Unsupervised clustering is based on the K -means method [33]. The results are evaluated using the best possible class mapping, that is, by checking the possible matchings between each cluster discovered and the target categories and selecting the matching that maximizes classification success. In practice, it can be assumed *a posteriori* that the samples taken near the (few) judges present during a Nordic Walking competition are correctly tagged. In this work, this tagging expansion leads to three class labels, c_0 , c_1 , and c_2 , corresponding respectively to correct practice, cheating, and incorrect practice.

ONLINE PROCESSING SUPERVISED CLASSIFICATION BASELINE

As a baseline, the following ML algorithms are applied, based on their good performance in HAR problems in the literature [16], [58], [59].

- **Gaussian Naive Bayes** (GNB) [60], based on a Gaussian distribution, for stream-based classification with the traditional Naive Bayes (NB) model.
- **Hoeffding Adaptive Tree Classifier** (HATC) [61], an online processing single tree-based model with a branch performance monitoring mechanism.
- **Adaptive Random Forest Classifier** (ARFC) [62], a stream-based tree ensemble majority voting with re-sampling and random feature selection using the concept drift mechanism.

The accuracy, precision (micro and macro), recall

(micro and macro), and elapsed time of these algorithms are calculated with the predictive sequential (*i.e.*, prequential evaluation) protocol for online processing learning [63].

EXPLAINABLE UNSUPERVISED RE-CLASSIFICATION

The explainability module traverses the estimator decision path of an ARFC model (also used as one of the supervised classification baseline algorithms) to extract the components of features $S_{p,a,s,l}^w[n] \forall w, p, a, s, l, \forall n > n_{init} = \max(w_{Q1}, w_{Q2}, w_{Q3}, w_{avg})$, which are all relevant for explainability purposes. The reclassification algorithm in this module is trained using tags c_0 , c_1 , and c_2 resulting from the clustering stage, which are translated to the class references available by expanding these references inside the corresponding clusters. Therefore, the clustering stage is explained from an interpretable ML algorithm with automatic unsupervised tagging because the tags are not manually produced. Let $S_{i,p,a,s,l}^w[n]$ be the i -th feature component, $i = 1..6$, of the 6-dimensional vector $S_{p,a,s,l}^w[n]$ defined from the metrics $Q_1^w[n]$, $Q_2^w[n]$, $Q_3^w[n]$, $avg^w[n]$, $std^w[n]$ and $F^w[n]$ in (3), in this same order. Note that, at slot n , a component will be only defined if its updated standard deviation exceeds threshold t_σ (for example, $S_{1,p,a,s,l}^w[n] = Q_{1,p,a,s,l}^w[n]$ when $Q_{1,p,a,s,l}^w[n] > t_\sigma$). Otherwise, it will be left undefined. In the sequel, undefined components are ignored in the calculations. Once the ARFC trees are obtained for the current prediction, all the paths leading to the corresponding class are traversed. Frequency $\xi_{i,p,a,s,l}^w[n]$ of subset $\{S_{i,p,a,s,l}^w[n], n \geq n_{init}\}$ is the number of times the tuple (i, w, p, a, s, l) is used as an index in those paths, as shown in Algorithm 1. The default feature component selected to display on the visual dashboard is $S_{i^*,p^*,a^*,s^*,l^*}^w[n]$, $(i^*, w^*, a^*, p^*, s^*, l^*) = \operatorname{argmax}_{(i,w,p,a,s,l)}(\xi_{i,p,a,s,l}^w[n])$, which becomes the first element of the ordered list $\Gamma[n]$. The rest of the elements in this list are components $\{S_{i,p,a,s,l}^w[n], n > n_{init}\}$ ordered in decreasing order of the frequencies taken from $\xi_{i,p,a,s,l}^w[n]$.

Visual content (feature values from six body sensors, further divided into three axes and four sliding windows) and textual descriptions (generated in natural language) of athlete performance are shown, together with predictions of practice type (correct, incorrect, and cheating).

EXPERIMENTAL RESULTS

This section describes the experimental data and wearable sensors used. Then, it outlines the different sub-problems in the tests, and finally, it presents and discusses the implementations and results observed for data calibration, feature engineering, analysis & selection, online processing baseline and unsupervised classification, and unsupervised explainability.

EXPERIMENTAL DATA

The NWGTI and PAMAP2 data sets were used to analyze the system's performance. NWGTI data were collected from training sessions involving five Nordic walkers under the guidance of Ignacio García Pérez, regional Nordic Walking coach of the Galician Mountaineering Federation, Spain. His expertise in technique and competition refereeing enabled the identification of correct practices and typical cases of incorrect practices and cheating, such as keeping the poles off the ground and pole dragging. The PAMAP2 data set⁵ was used for further evaluation and comparison purposes. This data set contains data on various physical activities, including Nordic Walking, and was also used by Wiktorski *et al.* (2019) [41].

Due to the streaming implementation, two types of data were used in the different sub-problems considered: raw data and engineered features from raw data.

- 1. Raw data. Up to 54 features were considered at each slot for the NWGTI data set, prior to feature engineering. These features directly corresponded to the sensor data available at the time (note that the sensors produce data at different rates, as described below). Forty features were extracted from the PAMAP2 data set. Note that each individual had three wearable IMUs: one on the chest and one each on the dominant wrist and dominant ankle. Each IMU included a temperature sensor, two tri-axial accelerometers, a tri-axial gyroscope, a tri-axial magnetometer, and a heart rate sensor, which was only activated on the chest.
- 2. Engineered features from raw data in the NWGTI and PAMAP2 data sets as described in the section METHODOLOGY. DATA CALIBRATION, FEATURE ENGINEERING, ANALYSIS & SELECTION.

⁵Available at <https://doi.org/10.24432/C5NW2H>, March 2024.

Algorithm 1: Extraction of relevant features

```
Data: classifier, prediction, sample // Output of the classification model.
Result: Relevant feature components sorted by frequency.
feature_list = []
for estimator in classifier do
    if prediction = estimator.predict(sample) then
        node = estimator[0] // Root node. Node structure:
        { feature, threshold, left_branch, right_branch, is_terminal_node }.
        while node[is_terminal_node]  $\neq$  True do
            feature = node[feature]
            threshold = node[threshold]
            if sample[feature]  $\leq$  threshold then
                node = node[left_branch]
            else
                feature_list.append(feature)
                node = node[right_branch]
            end
        end
    end
end
 $\Gamma[n]$  = feature_components_sorted_by_frequency(feature_list)
return  $\Gamma[n]$ 
```

WEARABLE SENSORS

As illustrated in Figure 2, six wearable IMUs by Mbientlab⁶ were used to collect the data for the NWGTI data. These IMUs comprised tri-axial accelerometers, gyroscopes, and magnetometers, with respective sampling rates of 12.5, 25, and 10 Hz. Their maximum admissible acceleration was 16 g. Our experiments showed a maximum acceleration excess of 4.75 g, which is within a reasonable margin and indicates adequate sensitivity.

Note that the different IMU sensors collected raw data at different rates. In principle thus, the assumption that all sensors are synchronized, implicit in the section METHODOLOGY. DATA CALIBRATION, FEATURE ENGINEERING, ANALYSIS & SELECTION, did not hold. The practical approach used to address this issue was to set “empty” $x_{p,a,s,l}[n]$ entries to NaN values at any input interrupt, which were ignored by feature computations (including online processing variability calculations).

Raw data from the 54 sensors available were produced during 12-minute average bursts. On average,

each burst consisted of 94 348 samples distributed as indicated in Table 2. The number of feature dimensions depended on the data type (raw or engineered), as explained in the section METHODOLOGY. DATA CALIBRATION, FEATURE ENGINEERING, ANALYSIS & SELECTION.

Table 2. Distribution of samples in the NWGTI data set from data bursts (average values).

Class	Number of samples
Correct practice	30 722
Cheating practice	33 330
Incorrect practice	30 296

The sampling rate for the PAMAP2 data set was 100 Hz, except for the heart rate sensor, which was 9 Hz. As previously mentioned, each IMU in this case had two tri-axial accelerometers with respective maximum admissible accelerations of 6 g and 16 g. Thus, their sensitivities were also adequate for our application. Only Nordic walkers who walked for at least 250 seconds or users who climbed stairs for at least 150 seconds. This resulted in 43 130 samples distributed as indicated in Table 3.

⁶Available at <https://www.bosch-sensortec.com/products/motion-sensors/imus/bmi160> and <https://mbientlab.com/store/metamotionrl>, March 2024.

Table 3. Distribution of samples in the PAMAP2 data set (average values).

Class	Number of samples
Nordic Walking	27 974
Climbing stairs	15 156

SUB-PROBLEMS

For baseline data, we performed online processing supervised classifications with prequential evaluation by predicting, testing, and training the model in this specific order. In all cases, data were decimated for training and testing. Training and testing were updated every ten slots for the NWGTI data set and, due to the higher sampling rate of 100 Hz, every 30 slots for the PAMAP2 data set.

- **A.** Baseline supervised classification of the samples of experimental engineered data (in the sequel, by sample we will refer to all or part of the available features at the corresponding slot).
- **B.** Baseline shuffled supervised classification: the samples of experimental engineered data of sub-problem A were partitioned into eight randomly shuffled subsets. This emulates a situation in which a person performs correctly or incorrectly or cheats at different moments compared to sub-problem A and shows that there are no long-term dependencies in the data.
- **C.** Baseline stressed supervised classification: the samples in sub-problem B were decimated again for training and testing. Thus, training and testing were applied with the 1/100 ratio. This sub-problem stresses online processing supervised classification to check its robustness when reducing the proportion of annotated data.
- **D.** Unsupervised explainable classification: sample clusters from sub-problem A were used for unsupervised explainable re-classification.

DATA CALIBRATION, FEATURE ENGINEERING, ANALYSIS & SELECTION

Data calibration. For the NWGTI data set, the calibration method in the section METHODOLOGY. DATA CALIBRATION, FEATURE ENGINEERING, ANALYSIS & SELECTION yielded on average $w_{avg} = 362 \pm 58$, $w_{Q1} = 168 \pm 0$, $w_{Q2} = 282 \pm 6$ and $w_{Q3} = 474 \pm 87$, once the sensors had been synchronized with NaN padding. For the PAMAP2 data set, $w_{avg} = 362 \pm 58$,

$w_{Q1} = 14 \pm 3$, $w_{Q2} = 19 \pm 5$ and $w_{Q3} = 25 \pm 5$.

Feature engineering. In the NWGTI data set, each engineered data sample had up to 24 features (the six features in Equation (3) for each of the four sliding windows) per sensor source, that is $24 \times 54 = 1296$ features, plus up to 54 additional features directly corresponding to sensor outputs available at that moment. Therefore, each engineered data sample had up to 1350 features at each slot. For the PAMAP2 data set, $24 \times 40 + 40 = 1000$ features in total were used. These resulted from the 40 raw sensor measurements and the 24 engineered features for each of these measurements. Table 4 details the features engineered per IMU for the two data sets.

Feature analysis & selection. The `VarianceThreshold`⁷ function from the `River`⁸ package was used to calculate online processed feature variances in the NWGTI data set and select those exceeding $t_{\sigma}^2 = 0.24 \pm 0.12$ in the raw data analysis and $t_{\sigma}^2 = 0.01 \pm 0.01$ in the engineered data scenario. This threshold was tuned as the median of the online processed variance of the features by considering the samples of a 60-second interval after the calibration stage. In the raw data analysis, at the last slot of the experiment, 27 ± 4 features were selected on average for sub-problems A, B, and C. The most relevant sensors were the accelerometers and the gyroscopes. In the case of engineered data, also at the last slot, 785 ± 69 features, of a total possible 1296 features were selected for sub-problems A and D. The average number of features selected for sub-problems B and C was 789 ± 59 . As in the case of raw data, the most relevant sensors were the accelerometers and the gyroscopes. The most relevant engineered feature was $F_{p,a,s,l}^w[n]$. In the PAMAP2 data set, the variance threshold was $t_{\sigma}^2 = 8.99 \pm 3.28$ in the raw data analysis and $t_{\sigma}^2 = 5.86 \pm 1.58$ in the engineered data scenario. In the raw data analysis,

⁷Available at <https://riverml.xyz/0.11.1/api/feature-selection/VarianceThreshold>, March 2024.

⁸Available at <https://riverml.xyz/0.11.1>, March 2024.

on average, 23 ± 2 features were selected for sub problem A and 23 ± 1 for problems B and C. In the engineered data analysis, the average number of features selected was 526 ± 32 for sub problems A and D and 525 ± 31 for sub problems B and C. The most important features were those related to accelerometers, magnetometers, and heart rate sensors. As with the NWGTI data set, the most relevant engineered feature was $F_{p,a,s,l}^w[n]$.

ONLINE PROCESSING BASELINE AND UNSUPERVISED CLASSIFICATION

The online processing supervised classification baseline algorithms were implemented with the GNB⁹, HATC¹⁰, ARFC¹¹, and *K*-means¹² libraries from the River package.

Listings 1, 2, and 3 respectively show the ranges for hyperparameter optimization (selected values in bold font) for the HATC, ARFC, and *K*-means models (the GNB model has no hyperparameters to tune). The ranges and best values were obtained experimentally using an *ad hoc* implementation of the GridSearch¹³ algorithm for data streams. Engineered data for sub-problem A was down-sampled by a factor of 100 to perform hyperparameter optimization. The selected hyperparameters for both data sets were the same for HATC and ARFC. For *K*-means, however, the selected values for *halflife* (which is related to centroid optimization) varied depending on the data set. For PAMAP2, the selected value within the specified sequence was 0.77 (not shown). Recall that the goal with this model was to discover three clusters for NWGTI and two for PAMAP2 (*i.e.*, *n_clusters* = 3 or 2).

Table 5 reports standard performance measurements by type of experimental data, sub-problem, and model (tags #1, #2, and #3 correspond to correct, cheating, and incorrect practices, respectively) for the NWGTI data set. It allows comparison between our unsupervised solution (scenario D with engineered features) and the supervised learning baselines (scenarios

Listing 1. HATC hyperparameter ranges and selected values in bold.

```
depth = [50, 100, 150]
tiethreshold = [0.5, 0.05, 0.005]
maxsize = [50, 100, 200]
```

Listing 2. ARFC hyperparameter ranges and selected values in bold.

```
models = [50, 100, 200]
features = [50, 100, 200]
lambda = [50, 100, 200]
```

A, B, and C, for both raw data and engineered features). All entries average the corresponding results for the user sessions in the experiments. Column “prequential time” is the total time needed to process all the samples for each model and sub-problem. It should be checked against the maximum data rate of the sensors, 25 Hz. In other words, for a method to be feasible in real-time, its prequential time per sample must be less than 40 ms (in our worst-case scenario, it is 3 ms, that is 306.35s divided by 94 348 samples, about 7.5 % of the limit value). It should be noted that all methods except *K*-means are used for obtaining baseline data due to their supervised nature, which is impractical for real use. Thus, in light of the results obtained, *K*-means is feasible.

First, it is interesting to observe that sub-problem A was highly separable when only raw data were used. The slowest method was ARFC, but it was also feasible in streaming mode. As expected, the results of sub-problem B suggest no long-term dependence. For sub-problem C, the outcome was considerably degraded, suggesting that, although the approaches seem robust, excessive decimation is not conducive to real-time operation on simple hardware since it compromises

Listing 3. *K*-means hyperparameter ranges and selected values in bold.

```
halflifenwgti = [0.05, 0.075, 0.1]
halflifepamap2 = [0.02:0.05:0.8]
mu = [0.01, 0.1, 1]
sigma = [0.001nwgti, 1, 10pamap2]
p = [1, 2]
```

⁹Available at <https://riverml.xyz/dev/api/naive-bayes/GaussianNB>, March 2024.

¹⁰Available at <https://riverml.xyz/0.13.0/api/tree/HoeffdingAdaptiveTreeClassifier>, March 2024.

¹¹Available at <https://riverml.xyz/dev/api/ensemble/AdaptiveRandomForestClassifier>, March 2024.

¹²Available at <https://riverml.xyz/0.11.1/api/cluster/KMeans>, March 2024.

¹³Available at https://scikit-learn.org/stable/modules/generated/sklearn.model_selection.GridSearchCV.html, March 2024.

Table 4. Raw and engineered (Eng.) features per IMU for the two data sets used.

Data set	ID	Name	Type
NWGTI	1-3	16g accelerometer axes	Raw
	4-6	Gyroscope axes	
	7-9	Magnetometer axes	
	10 - 225	$Q_1^w, Q_2^w, Q_3^w, avg^w, std^w$ and F^w for windows $w_{Q1}, w_{Q2}, w_{Q3}, w_{avg}$ for each sensor (1-9 above)	Eng.
PAMAP2	1-9	Same as features 1-9 of NWGTI data set	Raw
	10-12	6g accelerometer axes	
	13	Heart rate	
	14	Temperature	Eng.
	15 - 350	$Q_1^w, Q_2^w, Q_3^w, avg^w, std^w$ and F^w for windows $w_{Q1}, w_{Q2}, w_{Q3}, w_{avg}$ for each sensor (1-14 above)	

performance.

The performance gap between the different methods was reduced by introducing engineered data. The most relevant result here, highlighting the value of engineered data, was the significant improvement in sub-problem C, regardless of its low computational requirements. For this reason, we decided to test the practical, unsupervised approach of sub-problem D using engineered data. As shown in the last row of Table 5, performance was highly satisfactory, assuming each cluster is assigned to the correct class *a posteriori* to ensure minimum tagging. It should be noted that, in a competition scenario, it would not be necessary to determine which of the two differentiated incorrect behaviors corresponds to cheating and which to incorrect practice, since the correct practice cluster could be identified from the few points along the route where the practitioner passes by a judge. Moreover, a coach could differentiate them using training videos *a posteriori*.

After sub-problem D, with the inclusion of re-classification for explainability, the prequential processing time is the sum of the corresponding successive times of *K*-means and ARFC, that is, 224.15 ms, which is still feasible for real-time operation.

Table 6 shows the results obtained with the PAMAP2 data set. Although this data set is designed for activity differentiation not practice assessment (tags #1 and #2 correspond to Nordic Walking and stair climbing, respectively), the good performance achieved with our solution highlights the good quality of the data collected in NWGTI. The unsupervised model attained performance metrics above 90 % for Nordic Walking prediction, although the GNB classifier was the best model in this case. Elapsed times were considerably reduced due to the fewer samples and classes.

Figures 3 and 4 respectively show online changes in accuracy and cross entropy loss curves for scenario D (unsupervised learning) with the NWGTI data set. The accuracy was slightly reduced in the last two-thirds of the sequence, but it was still very good. To calculate the cross entropy loss graph we employed Equation (4), where E is the number of samples, M the number of classes, and h a one-hot encoded vector (in our experiment, as there exist three classes, if the sample corresponds to the second class, the vector was (0,1,0)), and $\rho_i[n]$ is the probability of predicting class i for the n -th sample). The graph showed a slight increase in accumulated error, but note that values lower than 0.5 are satisfactory given the logarithmic term in the *crloss* function.

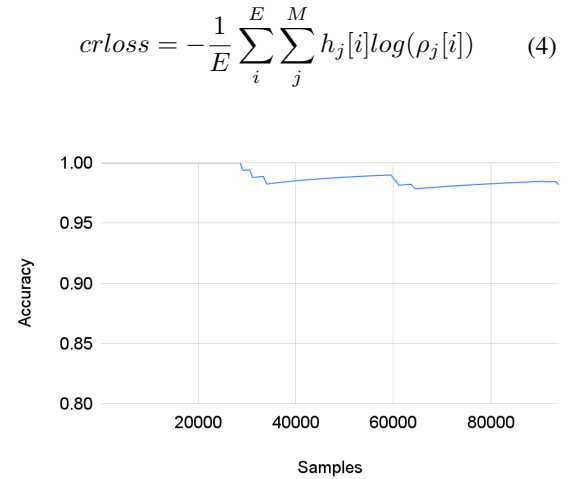


Figure 3. Accuracy curve for the NWGTI data set.

Finally, Table 7 compares our approach with the most closely related work in the literature. The authors, Derungs *et al.* (2018) [38], computed the same evaluation metrics in that work were computed, RMSE

Table 5. Online processing practice assessment results, NWGTI data set.

Data	Sce.	Model	Accuracy	Precision				Recall				Preq. time (s)
				Macro	#1	#2	#3	Macro	#1	#2	#3	
Raw	A	GNB	90.99 ± 7.04	91.86	93.27	93.38	88.93	91.15	94.45	90.30	88.71	1.79
		HATC	96.94 ± 1.80	97.19	97.90	95.75	97.92	96.90	98.38	98.84	93.47	3.07
		ARFC	99.03 ± 0.55	99.03	99.83	99.65	97.60	99.02	99.28	98.23	99.55	164.68
	B	GNB	79.87 ± 0.71	80.39	79.49	82.73	78.95	79.43	71.19	87.88	79.22	2.05
		HATC	92.98 ± 2.85	92.95	91.85	93.59	93.42	93.05	94.30	93.19	91.65	3.83
		ARFC	88.77 ± 4.39	89.00	83.38	91.45	92.16	88.76	91.97	91.06	83.25	306.35
	C	GNB	75.80 ± 2.31	76.14	73.28	82.31	72.84	75.26	65.49	84.75	75.53	1.87
		HATC	71.92 ± 11.63	71.52	67.08	74.89	72.57	71.25	64.50	83.25	66.00	1.50
		ARFC	70.46 ± 9.16	71.25	65.62	72.31	75.82	70.24	70.82	77.90	61.98	139.46
Eng.	A	GNB	95.39 ± 2.35	95.55	98.15	96.36	92.15	95.42	93.65	95.67	96.94	38.47
		HATC	93.53 ± 7.13	94.64	89.71	97.48	96.74	93.53	99.36	98.02	83.21	58.55
		ARFC	99.36 ± 0.31	99.38	99.59	99.21	99.33	99.36	99.91	99.44	98.74	178.02
	B	GNB	93.25 ± 4.55	93.40	89.79	96.23	94.20	93.13	95.17	94.03	90.20	42.56
		HATC	92.17 ± 2.64	92.34	91.87	94.46	90.68	92.21	93.93	93.10	89.61	83.36
		ARFC	98.79 ± 0.90	98.78	98.88	99.20	98.25	98.75	97.87	99.45	98.92	281.89
	C	GNB	92.44 ± 4.77	92.70	88.40	95.48	94.23	92.31	93.46	93.46	90.01	36.69
		HATC	91.05 ± 5.22	91.32	90.56	91.66	91.75	90.89	91.63	93.02	88.01	45.36
		ARFC	97.63 ± 0.66	97.58	97.12	98.52	97.09	97.61	97.32	97.54	97.97	117.57
	D	Clustering	97.68 ± 0.83	97.70	98.37	98.61	96.14	97.74	98.60	95.84	98.78	46.13

Table 6. Online processing practice assessment results, PAMAP2 data set.

Data	Sce.	Model	Accuracy	Precision			Recall			Preq. time (s)
				Macro	#1	#2	Macro	#1	#2	
Raw	A	GNB	95.69 ± 4.94	95.23	100.00	90.46	96.57	93.14	100.00	0.21
		HATC	82.74 ± 16.80	86.47	100.00	72.94	86.49	72.98	100.00	0.32
		ARFC	98.70 ± 0.67	98.25	100.00	96.49	98.98	97.96	100.00	16.90
	B	GNB	93.13 ± 4.71	92.33	95.98	88.67	93.15	93.09	93.21	0.22
		HATC	86.59 ± 6.32	85.96	87.63	84.28	83.89	92.76	75.01	0.41
		ARFC	87.08 ± 2.47	88.21	85.68	90.74	83.24	96.23	70.25	24.47
	C	GNB	90.33 ± 4.77	89.76	91.84	87.69	89.10	93.17	85.03	0.19
		HATC	80.04 ± 12.82	83.61	80.81	86.41	74.93	94.79	55.08	0.16
		ARFC	70.97 ± 6.65	70.08	72.27	67.89	63.18	89.96	36.40	10.44
Eng.	A	GNB	99.00 ± 0.21	98.62	100.00	97.24	99.23	98.46	100.00	3.61
		HATC	91.93 ± 10.43	92.35	100.00	84.69	93.85	87.70	100.00	6.02
		ARFC	96.99 ± 0.72	95.98	100.00	91.97	97.69	95.38	100.00	35.11
	B	GNB	99.27 ± 0.28	99.26	99.33	99.18	99.15	99.55	98.75	3.79
		HATC	95.87 ± 3.40	95.58	96.58	94.57	95.38	97.27	93.50	7.60
		ARFC	96.18 ± 2.71	96.00	96.62	95.38	95.64	97.51	93.77	66.65
	C	GNB	97.25 ± 0.60	97.42	97.00	97.83	96.54	98.81	94.27	3.17
		HATC	89.12 ± 11.57	92.50	87.32	97.68	85.40	99.35	71.45	3.21
		ARFC	96.59 ± 2.57	96.38	97.26	95.51	96.13	97.54	94.72	22.12
	D	Clustering	90.46 ± 11.39	93.57	92.26	94.88	87.97	95.53	80.41	3.40

and MAE. The lower error observed with our system can be explained by the fact that Derungs *et al.* (2018) [38] only considered classifiers as regressors and did not use nominal categories, which we used to explore strategies such as the ARFC model. Furthermore, they grouped sensor data into individual strides, preventing continuous signal analysis. Finally, this comparison must be understood as a reference since the approach in Derungs *et al.* [38] was supervised, and our premise was to avoid that limitation to the greatest possible extent.

Table 7. Comparison with the most related work.

Approach	RMSE	MAE
This work on NWGTI	0.18	0.03
Derungs <i>et al.</i> (2018) [38]	0.43	0.18

UNSUPERVISED EXPLAINABILITY

The ARFC algorithm is the basis for explainability once trained with the clusters returned by the online processing unsupervised *K*-means algorithm. It is based on the Hoeffding tree model [62]. The explainability module groups the trees from the ARFC model by predicted categories. Then, the River

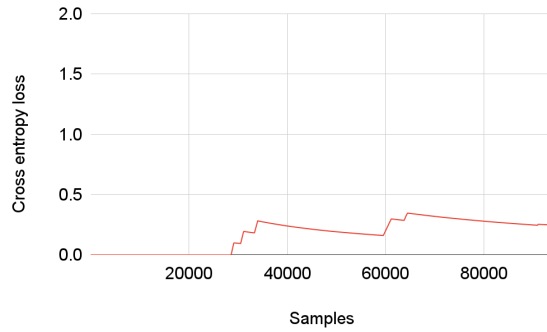


Figure 4. Cross entropy loss curve for the NWGTI data set.

debug_one ARFC method¹⁴ is used to extract the decision paths traversed, whose features are stored in lists. The lists are then combined, and the frequency with which feature components appear is calculated as explained in the section EXPLAINABLE UNSUPERVISED RE-CLASSIFICATION. At this point, the feature components are ranked in decreasing order of relevance. In Figure 5, the most representative feature component to that point, corresponding to the z -axis of the right wrist accelerometer and the w_{Q1} sliding window of the Q_2^w component, is displayed. Other feature components can be selected for display using the drop box on the dashboard.

The dashboard was designed with TEMPLATED¹⁵ and its charts with Highcharts¹⁶. Figure 5 shows an automatic explanation of a training session of one of the Nordic Walking practitioners in our experiments.

The upper part shows the selected sensor as previously defined. The real-time graph for the sensor is shown on the left, where green, purple, and blue identify correct, cheating, and incorrect practices, respectively. The description of the latest prediction in natural language, based on the ARFC decision path, is the text in the bottom left corner, corresponding to the tree path displayed in the bottom right corner. The extracted information is introduced into natural language templates taken from Listing 4 (where ellipses indicate that the immediately preceding text is repeated as needed). Our system follows the tree path of the latest prediction and extracts all associated index tuples (a, s) . In case of repetition, an index tuple (a, s) is only considered

Listing 4. Explainability templates.

#1 The [component list] value<s> of the [axis] [sensor] within the [windows list] window<s> and ... define the decision path.

#2 The component<s> identified suggest that the value<s> remain stable in the [sensor] case.

#3 In the case of the [sensor] a change in the [component] in the last samples and ... produce<s> the prediction of [correct/cheating/incorrect] practice.

#4 Moreover, a cheating practice was detected between [start time] and [end time]; the last detected sample prediction corresponds to [correct/cheating/incorrect] practice with [confidence] confidence.

once. For each instance, template #1 is updated with the lists of different components and windows across the decision path corresponding to the selected tuples. Template #2 is applied to all nodes along the decision path in which the ' \leq ' condition holds for a component whose updated standard deviation is less than t_σ . For each node along the tree path, template #3 is updated whenever a ' $>$ ' condition holds for the sensor and component considered in that node. Finally, template #4 identifies the cheating interval, if present, and the current prediction, including its confidence interval.

The w_{Q1} , w_{Q2} , w_{Q3} , and w_{avg} windows determine the time duration under analysis. When the features in the decision path displayed in the dashboard correspond to the w_{Q1} window (as in the example), the value changes are recent. Features corresponding to the w_{Q3} window, by contrast, are more spaced in time. The Q_1^w , Q_2^w , Q_3^w , avg^w , std^w , and F^w features allow for the interpretation of extreme values. Specifically, a value in Q_1^w would indicate that only 25% of the samples have lower values. F^w indicates a change in the trend of the movement. The prediction confidence was obtained using the ARFC predict_proba_one method. This information is

¹⁴ Available at <https://riverml.xyz/0.14.0/api/tree/HoeffdingTreeClassifier>, March 2024.

¹⁵ Available at <https://templated.co>, March 2024.

¹⁶ Available at <https://www.highcharts.com>, March 2024.

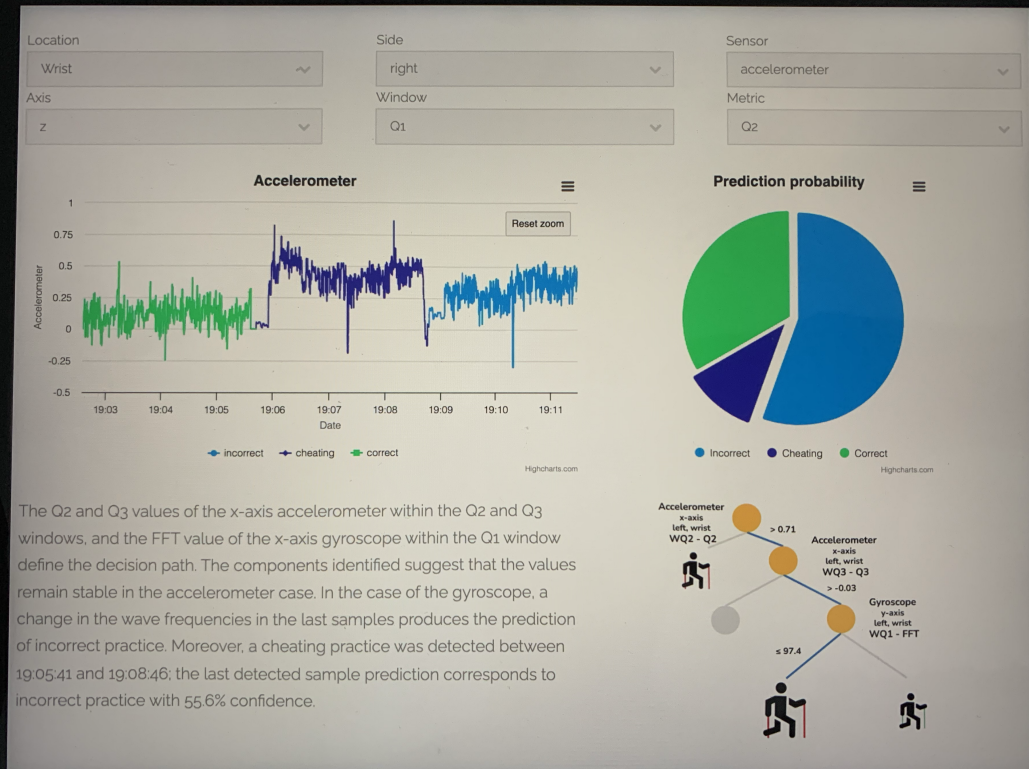


Figure 5. Screenshot of explainability dashboard.

displayed graphically in the tree in the bottom right of the image in Figure 5.

CONCLUSIONS

Evaluation of sport and physical activity, including aspects such as performance monitoring and injury prevention, is a major field of application for AI HAR techniques. ML-based solutions are helpful for differentiating between well-defined states within large volumes of data collected using inexpensive portable sensors such as wearables and smartphones. Unsupervised techniques are very interesting in this context as they can be used in the design of stand-alone systems. Nordic Walking HAR, the core application of this research, aligns well with these assumptions, and can be used to differentiate between correct and incorrect techniques and practices that would result in disqualification. This information would be useful for practitioners, trainers, and competition judges.

In the proposed solution, supervised (baseline) and unsupervised models were trained using data from

wearable inertial sensors. These data were then augmented using data engineering techniques to allow long processing slots. Experimental testing demonstrated the appropriateness of the unsupervised learning approach, as it achieved a classification accuracy of close to 100 % (note that the experimental evaluation also considered an alternative data set from the literature and showed that our data collection was not biased toward improving performance results). The outcome of the unsupervised learning stage (*i.e.*, the resulting clusters) yields labels at minimal cost for automatic explainable re-classification. By reducing thus the need for laborious manual tagging, without compromising interpretability, our work contributes to solving a common need in HAR for consumer electronics applications.

The automatic explanations generated for the classification results include textual and visual descriptions of athletes' performance as well as intelligible explanations of the predictions made by the ML models. The ultimate objective is to promote trust, transparency, and

acceptance for AI solutions.

Automatic explainability has received very little attention in sports to date, with solutions focusing on offline supervised approaches. To our knowledge, our system is the first solution to combine online processing, explainability, and unsupervised assessment for HAR in the field of sport. The flexible positioning of the data collection sensors is an additional advantage of our approach.

Currently, use of our system is limited to sports or training practices with clearly defined patterns or stages, such as martial arts kata training, boxing bag exercises, certain forms of gymnastics (*e.g.*, rings), and, as shown in this paper, Nordic Walking. Future work is needed to extend its application to more open, “fluid”, sports, such as soccer and basketball. In addition, when applicable, we plan to take advantage of the solution’s modular design to include a reinforcement learning module based on the *human in the loop* approach. This would allow experts to provide feedback to continually improve the system and its performance.

ACKNOWLEDGMENTS

This work was partially supported by Xunta de Galicia grants ED481B-2021-118, ED481B-2022-093, and ED431C 2022/04, Spain. The authors are indebted to Nordic Walking Vigo and Mr. Ignacio García Pérez for their help obtaining representative experimental data for correct, incorrect, and cheating practices.

REFERENCES

1. C. Jobanputra, J. Bavishi, and N. Doshi, “Human Activity Recognition: A Survey,” *Procedia Comput. Sci.*, vol. 155, pp. 698–703, 2019.
2. M. Al-Hammadi, G. Muhammad, W. Abdul, M. Alsulaiman, and M. S. Hossain, “Hand Gesture Recognition Using 3D-CNN Model,” *IEEE Consum. Electron. Mag.*, vol. 9, pp. 95–101, 2020.
3. A. Ayman, O. Attalah, and H. Shaban, “An Efficient Human Activity Recognition Framework Based on Wearable IMU Wrist Sensors,” in *Proceedings of the IEEE International Conference on Imaging Systems and Techniques*. IEEE, 2019, pp. 1–5.
4. S. Abbaspour, F. Fotouhi, A. Sedaghatbaf, H. Fotouhi, M. Vahabi, and M. Linden, “A Comparative Analysis of Hybrid Deep Learning Models for Human Activity Recognition,” *Sensors*, vol. 20, no. 19, pp. 5707–5720, 2020.
5. F. Bozkurt, “A Comparative Study on Classifying Human Activities Using Classical Machine and Deep Learning Methods,” *Arab. J. Sci. Eng.*, vol. 47, no. 2, pp. 1507–1521, 2022.
6. J. W. Navalta, J. Montes, N. G. Bodell, C. D. Aguilar, K. Radzak, J. W. Manning, and M. DeBeliso, “Reliability of Trail Walking and Running Tasks Using the Stryd Power Meter,” *Int. J. Sports Med.*, vol. 40, no. 8, pp. 498–502, 2019.
7. E. T. Mohamad, D. J. Armaghani, E. Momeni, A. H. Yazdavar, and M. Ebrahimi, “Rock strength estimation: a PSO-based BP approach,” *Neural Comput. Appl.*, vol. 30, no. 5, pp. 1635–1646, 2018.
8. S. K. Challa, A. Kumar, and V. B. Semwal, “A multibranch CNN-BiLSTM model for human activity recognition using wearable sensor data,” *Vis. Comput.*, p. 4095–4109, 2021.
9. E. E. Cust, A. J. Sweeting, K. Ball, and S. Robertson, “Machine and deep learning for sport-specific movement recognition: a systematic review of model development and performance,” *J. Sports Sci.*, vol. 37, no. 5, pp. 568–600, 2019.
10. D. Borms and A. Cools, “Upper-Extremity Functional Performance Tests: Reference Values for Overhead Athletes,” *Int. J. Sports Med.*, vol. 39, no. 6, pp. 433–441, 2018.
11. X. Hu, S. Mo, and X. Qu, “Basketball Activity Classification Based on Upper Body Kinematics and Dynamic Time Warping,” *Int. J. Sports Med.*, vol. 41, pp. 255–263, 2020.
12. S. S. Tabrizi, S. Pashazadeh, and V. Javani, “A Deep Learning Approach for Table Tennis Forehand Stroke Evaluation System Using an IMU Sensor,” *Comput. Intell. Neurosci.*, vol. 2021, pp. 1–15, 2021.
13. J. Vales-Alonso, D. Chaves-Diéguez, P. López-Matencio, J. J. Alcaraz, F. J. Parrado-García, and F. J. González-Castaño, “SAETA: A Smart Coaching Assistant for Professional Volleyball Training,” *IEEE Trans. Syst. Man Cybern.*, vol. 45, no. 8, pp. 1138–1150, 2015.
14. L. Lerebourg, D. Saboul, M. Cléménçon, and J. B. Coquart, “Prediction of Marathon Performance using Artificial Intelligence,” *Int. J. Sports Med.*, pp. 352–360, 2022.
15. L. Bai, C. Yeung, C. Efstratiou, and M. Chikomo, “Motion2Vector: unsupervised learning in human activity recognition using wrist-sensing data,” in *Proceedings of the ACM International Joint Conference on Pervasive and Ubiquitous Computing and Proceedings of the ACM International Symposium*

- on *Wearable Computers*. Association for Computing Machinery, 2019, pp. 537–542.
16. J. Shen and H. Fang, “Human Activity Recognition Using Gaussian Naïve Bayes Algorithm in Smart Home,” *J. Phys. Conf. Ser.*, vol. 1631, no. 1, pp. 012 059–012 064, 2020.
 17. C. Bulac and A. Bulac, “Decision Trees,” in *Advanced Solutions in Power Systems: HVDC, FACTS, and Artificial Intelligence*. Wiley, 2016, pp. 819–844.
 18. D. A. Pisner and D. M. Schnyer, “Support vector machine,” in *Machine Learning*. Elsevier, 2020, pp. 101–121.
 19. P. Cunningham and S. J. Delany, “k-Nearest Neighbour Classifiers - A Tutorial,” *ACM Comput. Surv.*, vol. 54, no. 6, pp. 1–25, 2022.
 20. B. Pavlyshenko, “Using Stacking Approaches for Machine Learning Models,” in *Proceedings of the IEEE International Conference on Data Stream Mining & Processing*. IEEE, 2018, pp. 255–258.
 21. M. H. M. Noor, Z. Salcic, and K. I. Wang, “Adaptive sliding window segmentation for physical activity recognition using a single tri-axial accelerometer,” *Pervasive Mob. Comput.*, vol. 38, pp. 41–59, 2017.
 22. E. Bulbul, A. Cetin, and I. A. Dogru, “Human Activity Recognition Using Smartphones,” in *Proceedings of the International Symposium on Multidisciplinary Studies and Innovative Technologies*. IEEE, 2018, pp. 1–6.
 23. M. N. S. Zainudin, M. N. Sulaiman, N. Mustapha, and T. Perumal, “Activity Recognition Using One-Versus-All Strategy with Relief-F and Self-Adaptive Algorithm,” in *Proceedings of the IEEE Conference on Open Systems*. IEEE, 2018, pp. 31–36.
 24. P. Bharti, D. De, S. Chellappan, and S. K. Das, “HuMAN: Complex Activity Recognition with Multi-Modal Multi-Positional Body Sensing,” *IEEE Trans. Mob. Comput.*, vol. 18, no. 4, pp. 857–870, 2019.
 25. M. Gil-Martín, R. San-Segundo, F. Fernández-Martínez, and R. de Córdoba, “Human activity recognition adapted to the type of movement,” *Comput. Electr. Eng.*, vol. 88, pp. 106 822–106 835, 2020.
 26. P. Zhu and F. Sun, “Sports Athletes’ Performance Prediction Model Based on Machine Learning Algorithm,” in *Advances in Intelligent Systems and Computing*. Springer, 2020, vol. 1017, pp. 498–505.
 27. A. Rossi, L. Pappalardo, and P. Cintia, “A Narrative Review for a Machine Learning Application in Sports: An Example Based on Injury Forecasting in Soccer,” *Sports*, vol. 10, no. 1, pp. 5–20, 2021.
 28. M. Webber and R. F. Rojas, “Human Activity Recognition With Accelerometer and Gyroscope: A Data Fusion Approach,” *IEEE Sens. J.*, vol. 21, no. 15, pp. 16 979–16 989, 2021.
 29. Y. Zeng, C. Wang, C.-C. Chen, W.-P. Xiong, Z. Liu, Y.-C. Huang, and C. Shen, “Smart Device Monitoring System Based on Multi-type Inertial Sensor Machine Learning,” *Sens. Mater.*, vol. 33, no. 2, pp. 693–714, 2021.
 30. L. Zhang and N. Li, “Material analysis and big data monitoring of sports training equipment based on machine learning algorithm,” *Neural Comput. Appl.*, vol. 34, no. 4, pp. 2749–2763, 2022.
 31. J. Suto and S. Oniga, “Efficiency investigation of artificial neural networks in human activity recognition,” *J. Ambient. Intell. Humaniz. Comput.*, vol. 9, no. 4, pp. 1049–1060, 2018.
 32. C. Domingo, S. See, and R. Legaspi, “Unsupervised Habitual Activity Detection in Accelerometer Data,” in *Mechatronics and Machine Vision in Practice 3*, 2018, pp. 253–272.
 33. K. P. Sinaga and M.-S. Yang, “Unsupervised K-Means Clustering Algorithm,” *IEEE Access*, vol. 8, pp. 80 716–80 727, 2020.
 34. J. Gu, Z. Wang, J. Kuen, L. Ma, A. Shahroudy, B. Shuai, T. Liu, X. Wang, G. Wang, J. Cai, and T. Chen, “Recent advances in convolutional neural networks,” *Pattern Recognit.*, vol. 77, pp. 354–377, 2018.
 35. D. van Kuppevelt, J. Heywood, M. Hamer, S. Sabia, E. Fitzsimons, and V. van Hees, “Segmenting accelerometer data from daily life with unsupervised machine learning,” *Plo ONE*, vol. 14, no. 1, pp. e0 208 692–e0 208 710, 2019.
 36. R. Janarthanan, S. Doss, and S. Baskar, “Optimized unsupervised deep learning assisted reconstructed coder in the on-nodule wearable sensor for human activity recognition,” *Measurement*, vol. 164, pp. 108 050–108 060, 2020.
 37. C. Serantoni, G. Zimatore, G. Bianchetti, A. Abeltino, M. D. Spirito, and G. Maulucci, “Unsupervised Clustering of Heartbeat Dynamics Allows for Real Time and Personalized Improvement in Cardiovascular Fitness,” *Sensors*, vol. 22, pp. 3974–3969, 2022.
 38. A. Derungs, S. Soller, A. Weishaupl, J. Bleuel, G. Berschin, and O. Amft, “Regression-based, mistake-driven movement skill estimation in Nordic Walking using wearable inertial sensors,” in

- Proceedings of the IEEE International Conference on Pervasive Computing and Communications.* IEEE, 2018, pp. 1–10.
39. F. Mocera, G. Aquilino, and A. Somà, “Nordic Walking Performance Analysis with an Integrated Monitoring System,” *Sensors*, vol. 18, no. 5, pp. 1505–1517, 2018.
 40. P. Pierleoni, S. Raggiunto, S. Marzorati, L. Palma, A. Cucchiarelli, and A. Belli, “Activity Monitoring Through Wireless Sensor Networks Embedded Into Smart Sport Equipments: The Nordic Walking Training Utility,” *IEEE Sens. J.*, vol. 22, no. 3, pp. 2744–2757, 2022.
 41. T. Wiktorski and J. C.-W. Lin, “Approximate Approach to Finding Generic Utility of Sequential Patterns,” in *Proceedings of the International Conference on Data Mining Workshops.* IEEE, 2019, pp. 1029–1034.
 42. P. Kumar, R. Kumar, M. Aloqaily, and A. K. M. N. Islam, “Explainable AI and Blockchain for Metaverse: A Security, and Privacy Perspective,” *IEEE Consum. Electron. Mag.*, pp. 1–7, 2023.
 43. F. de Arriba-Pérez, S. García-Méndez, F. J. González-Castaño, and J. González-González, “Explainable machine learning multi-label classification of Spanish legal judgements,” *J. King Saud Univ. Comput. Inf. Sci.*, pp. 10 180–10 192, 2022.
 44. J. González-González, S. García-Méndez, F. De Arriba-Pérez, F. J. González-Castaño, and Ó. Barba-Seara, “Explainable Automatic Industrial Carbon Footprint Estimation From Bank Transaction Classification Using Natural Language Processing,” *IEEE Access*, vol. 10, pp. 126 326–126 338, 2022.
 45. M. Ehatisham-ul Haq, M. N. Malik, M. A. Azam, U. Naeem, A. Khalid, and M. A. Ghazanfar, “Identifying Users with Wearable Sensors based on Activity Patterns,” *Procedia Comput. Sci.*, vol. 177, pp. 8–15, 2020.
 46. Y. Wang, W. Liu, and X. Liu, “Explainable AI techniques with application to NBA gameplay prediction,” *Neurocomputing*, vol. 483, pp. 59–71, 2022.
 47. C. Feely, B. Caulfield, A. Lawlor, and B. Smyth, “Providing Explainable Race-Time Predictions and Training Plan Recommendations to Marathon Runners,” in *Proceedings of the ACM Conference on Recommender Systems.* Association for Computing Machinery, 2020, pp. 539–544.
 48. X. Sun, J. Davis, O. Schulte, and G. Liu, “Cracking the Black Box,” in *Proceedings of the ACM SIGKDD International Conference on Knowledge Discovery & Data Mining.* Association for Computing Machinery, 2020, pp. 3154–3162.
 49. G. Lisca, C. Prodaniuc, T. Grauschopf, and C. Axenie, “Less Is More: Learning Insights From a Single Motion Sensor for Accurate and Explainable Soccer Goalkeeper Kinematics,” *IEEE Sens. J.*, vol. 21, no. 18, pp. 20 375–20 387, 2021.
 50. S. García-Méndez, F. Leal, B. Malheiro, J. C. Burguillo-Rial, B. Veloso, A. E. Chis, and H. González-Vélez, “Simulation, modelling and classification of wiki contributors: Spotting the good, the bad, and the ugly,” *Simul. Model. Pract. Theory*, vol. 120, pp. 102 616–102 628, 2022.
 51. H. Bi, M. Perello-Nieto, R. Santos-Rodriguez, and P. Flach, “Human Activity Recognition Based on Dynamic Active Learning,” *IEEE J. Biomed. Health Inform.*, vol. 25, pp. 922–934, 2021.
 52. B. Fu, N. Damer, F. Kirchbuchner, and A. Kuijper, “Sensing Technology for Human Activity Recognition: A Comprehensive Survey,” *IEEE Access*, vol. 8, pp. 83 791–83 820, 2020.
 53. Z. Meng, M. Zhang, C. Guo, Q. Fan, H. Zhang, N. Gao, and Z. Zhang, “Recent Progress in Sensing and Computing Techniques for Human Activity Recognition and Motion Analysis,” *Electronics*, vol. 9, pp. 1357–1375, 2020.
 54. N. Herencsar, “AI-Empowered Next Generation Consumer Internet of Things,” *IEEE Consum. Electron. Mag.*, vol. 12, pp. 11–13, 2023.
 55. S. Edwards, S. White, S. Humphreys, R. Robergs, and N. O’Dwyer, “Caution using data from triaxial accelerometers housed in player tracking units during running,” *J. Sports Sci.*, vol. 37, no. 7, pp. 810–818, 2019.
 56. S. O. Slim, A. Atia, M. M.A., and M.-S. M. Mostafa, “Survey on Human Activity Recognition based on Acceleration Data,” *Int. J. Adv. Comput. Sci. Appl.*, vol. 10, no. 3, pp. 84–98, 2019.
 57. M. Stuart and M. Manic, “Deep Learning Shared Bandpass Filters for Resource-Constrained Human Activity Recognition,” *IEEE Access*, vol. 9, pp. 39 089–39 097, 2021.
 58. M. Khannouz and T. Glatard, “A Benchmark of Data Stream Classification for Human Activity Recognition on Connected Objects,” *Sensors*, vol. 20, pp. 6486–6502, 2020.
 59. D. Chen, S. Yongchareon, E. M.-K. Lai, Q. Z. Sheng, and V. Liesaputra, “Locally Weighted Ensemble-Detection-Based Adaptive Random Forest Classifier for Sensor-Based Online Activity Recognition for Multiple Residents,” *IEEE Internet Thing J.*, vol. 9, pp. 13 077–13 085, 2022.

60. Q. Xue, Y. Zhu, and J. Wang, "Joint Distribution Estimation and Naïve Bayes Classification Under Local Differential Privacy," *IEEE Trans. Emerg. Top. Comput.*, vol. 9, no. 4, pp. 2053–2063, 2021.
61. M. Stirling, Y. S. Koh, P. Fournier-Viger, and S. D. Ravana, "Concept Drift Detector Selection for Hoeffding Adaptive Trees," in *Lecture Notes in Computer Science (including subseries Lecture Notes in Artificial Intelligence and Lecture Notes in Bioinformatics)*. Springer, 2018, vol. 11320 LNAI, pp. 730–736.
62. H. M. Gomes, A. Bifet, J. Read, J. P. Barddal, F. Enembreck, B. Pfahringer, G. Holmes, and T. Abdessalem, "Adaptive random forests for evolving data stream classification," *Mach. Learn.*, vol. 106, no. 9-10, pp. 1469–1495, 2017.
63. J. Gama, R. Sebastião, and P. P. Rodrigues, "On Evaluating Stream Learning Algorithms," *Mach. Learn.*, vol. 90, no. 3, pp. 317–346, 2013.

Silvia García-Méndez received a Ph.D. in Information and Communication Technologies from the University of Vigo in 2021. Since 2015, she has worked as a researcher with the Information Technologies Group at the University of Vigo. She is collaborating with foreign research centers as part of her post-doctoral stage. Her research interests include Natural Language Processing techniques and Machine Learning algorithms.

Francisco de Arriba-Pérez received a B.S. degree in telecommunication technologies engineering in 2013, an M.S. degree in telecommunication engineering in 2014, and a Ph.D. degree in 2019 from the University of Vigo, Spain. He is currently a researcher in the Information Technologies Group at the University of Vigo, Spain. His research includes the development of Machine Learning solutions for different domains like finance and health.

Francisco J. González-Castaño received a B.S. degree from the University of Santiago de Compostela, Spain, in 1990 and a Ph.D. degree from the University of Vigo, Spain, in 1998. He is a full professor at the University of Vigo, Spain, leading the Information Technologies Group. He has authored over 120 papers in international journals in the fields of telecommunications and computer science and has participated in several relevant national and international projects. He holds three U.S. patents.

Javier Vales-Alonso received a degree in telecommunication engineering from the Universidad de Vigo, Spain, in 2000, the M.Sc. degree in mathematics from the Universidad Nacional de Educación a Distancia, Spain, in 2005, and the Ph.D. degree in computer science from the Universidad Politécnica de Cartagena (UPCT), Spain, in 2015, where he is currently a Full Professor with the Department of Information and Communication Technologies. He is involved in different research topics related to modeling and optimization.